Low-Energy Electron-Stimulated Luminescence of Thin H_2O and D_2O Layers on Pt(111)

Nikolay G. Petrik and Greg A. Kimmel*

Fundamental Science Directorate, Pacific Northwest National Laboratory, Mail Stop K8-88, P.O. Box 999, Richland, Washington 99352

Received: December 29, 2004; In Final Form: April 11, 2005

The electron-stimulated luminescence (ESL) from amorphous solid water and crystalline ice films deposited on Pt(111) at 100 K is investigated as a function of the film thickness, incident electron energy (5−1000 eV), isotopic composition, and film structure. The ESL emission spectrum has a characteristic double-peaked shape that has been attributed to a transition between a superexcited state ($\tilde{C}$) and the dissociative, first excited state ($\tilde{A}$) in water: $\tilde{C} \rightarrow \tilde{A}$. Comparing the electron-stimulated luminescence and O_2 electron-stimulated desorption (ESD) yields versus incident electron energy, we find the ESL threshold is ∼3 eV higher than the O_2 ESD threshold, which is close to the center of the emission spectrum near 400 nm and supports the $\tilde{C} \rightarrow \tilde{A}$ assignment for the ESL. For thin films, radiative and nonradiative interactions with the substrate tend to quench the luminescence. The luminescence yield increases with coverage since the interactions with the substrate become less important. The ESL yield from D_2O is ∼4−5 times higher than that from H_2O. With use of layered films of H_2O and D_2O, this sizable isotopic effect on the ESL is exploited to spatially profile the luminescence emission within the ASW films. These experiments show that most of the luminescence is emitted from within the penetration depth of the incident electron. However, the results depend on the order of the isotopes in the film and can be modeled by assuming some migration of the electronically excited states within the film. The ESL is very sensitive to defects and structural changes in solid water, and the emission yield is significantly higher from amorphous films than from crystalline ice.

I. Introduction

High-energy radiation (γ-rays, α particles, X-rays, etc.) produces cascades of low-energy secondary electrons in condensed matter, and the subsequent reactions of these low-energy electrons cause most of the chemical and physical changes in aqueous systems. The mechanisms of these electron-driven processes in water have been characterized in research over the last several decades.[1] More recently, the interactions of condensed water with low-energy electrons[2−8] have been studied and a variety of nonthermal reaction mechanisms have been identified. There are three major primary processes that can cause chemical changes in condensed water under electron irradiation: ionization, direct excitation, and dissociative electron attachment.[3,5,9−11] The primary processes and the final "bond-breaking" events can be well separated in space. Recent experiments[6,8] have shown that electron-stimulated reactions in thin ASW films occur preferentially at or near the ASW/vacuum *and* Pt/ASW interfaces. However, the energy driving these reactions can migrate through the films over long distances, e.g. up to ∼150 nm corresponding to 400 monolayers (ML). The mechanisms for the energy migration are not well understood. Similar energy transfer was observed in alkali halides and rare gas solids, where the location of an initial electron excitation and the subsequent reactions can also be spatially separated.[12−14] In those cases, excitons created in the bulk can diffuse to the vacuum interfaces where they subsequently lead to desorption, and a similar mechanism might occur in water.

Investigating the nonthermal luminescence can also provide insight into the mechanisms of energy transfer and relaxation in aqueous systems. For example, the radioluminescence of crystalline water ice has been studied with 50 keV X-rays,[15−19] high-energy (>0.5 MeV) electrons,[20−25] and low-energy (<200 eV) electrons.[26,27] Despite this level of effort, there are many models in the literature and no unified picture has emerged to reconcile the available data. All the experiments show a complicated luminescence emission spectrum with a main broad peak near 400 ± 30 nm (fwhm = 70−90 nm) and two minor peaks around 280−300 and 500−550 nm. The 300-nm emission has been assigned to the ($\tilde{A}^2\Sigma^+ \rightarrow \tilde{X}^2\Pi$) fluorescence of excited OH radicals—products of water dissociation trapped in the ice.[27] The nature of the main emission band near 400 nm is not yet clear and several mechanisms have been proposed: electron−ion recombination leading to creation of various excited states of water ($^3B_2$, $^1B_1$, $^3B_1$),[27,28] or $H^+ + OH^-$ recombination leading to creation of the C^1B_1 state,[23] or recombination of electrons with impurity cations,[15] or phosphorescence of OH radicals.[26] The shape of the 400 nm emission band is typically a broad Gaussian, but some experiments show a resolved multipeak structure.[23,27] The ∼500 nm emission source is also not clear, but was tentatively associated with the $\tilde{D}^1A_1$ state of water.[27]

Experiments with low-energy electron irradiation show luminescence thresholds at ∼9 eV[26,27] for the 300 nm band and at ∼10 eV [27]or ∼12 eV [26] for the 400 nm band. The luminescence thresholds have been attributed to the thresholds for dissociation and to ionization of water molecules in ice. Several experimental observations suggest involvement of precursors or defects in the main 400 nm emission process: (i) the luminescence yield increased with irradiation dose for 0.5 MeV electrons and 50 keV X-rays;[15,19,20] and (ii) 400 nm emission was detected in the photon-stimulated luminescence of preirradiated ice samples,[28,29] as well as in the afterglow

* Address correspondence to this author. E-mail: gregory.kimmel@pnl.gov.

10.1021/jp044077b CCC: $30.25 © 2005 American Chemical Society
Published on Web 08/04/2005

spectra of ices.[18] A significant isotopic effect has been observed for H_2O and D_2O samples where luminescence yields from D_2O were 4−10 times higher,[18,19,27] probably due to the difference in the quenching of the excited state responsible for the luminescence. In D_2O/H_2O mixtures, the luminescence yield is reduced to levels near that for pure H_2O even at low H_2O concentrations.[19] Many impurities in ice affect the 400 nm emission yield significantly, even at low concentrations (e.g. $10^{-4}-10^{-3}$ mol/L). For example, alkali halide salts, HCl, and alkali hydroxides enhance the luminescence by up to an order of magnitude, but hydrogen peroxide suppresses it.[15,19]

Here we investigate the electron-stimulated luminescence (ESL) from thin water films of D_2O and H_2O grown on Pt(111) as a function of the film thickness, incident electron energy (5−1000 eV), isotopic composition, and structure. The ESL emission spectrum is centered near 400 nm and has a double-peaked shape characteristic of the $\tilde{C} \rightarrow \tilde{A}$ transition in molecular water (superexcited state to lowest excited state).[30] This assignment is supported by comparing the ESL and O_2 electron-stimulated desorption (ESD) yields versus incident electron energy: The ESL and O_2 ESD thresholds are close to the expected energy levels for the $\tilde{C}$ and $\tilde{A}$ states, respectively, and the ∼3 eV energy difference between the thresholds corresponds to the photon energy at the maximum of the ESL emission spectrum. For thin films, the ESL intensity is reduced by interactions with the metal substrate and it increases with increasing film thickness. The ESL yield from D_2O is ∼4−5 times higher than that from H_2O. The isotopic effect is used in conjunction with layered films of H_2O and D_2O to determine the spatial profile of the ESL within the films. We find that most of the luminescence is emitted from within the penetration depth of the incident electrons. However, the results depend on the order of the isotope layers (i.e., D_2O on top or H_2O on top). The results can be explained if the electronic excitations responsible for the luminescence can migrate a short distance prior to emission. The ESL is also very sensitive to structural changes in solid water as seen from the significant difference of emission yields from ASW and crystalline ice.

II. Experimental Section

The experiments were performed in an ultrahigh vacuum (UHV) system, equipped with a low-energy electron gun (Kimball Physics ELG-2), a liquid nitrogen-cooled cryostat, two effusive gas dosers for growing thin films of H_2O and D_2O, and a quadrupole mass spectrometer (QMS) with line-of-sight detection geometry.[6] Typical base pressures for the system were $\sim 3 \times 10^{-10}$ Torr. The polished platinum single crystal (Princeton Scientific Corp.) was 10 mm in diameter and 1 mm thick, and was cut to within ±0.5° of the (111) surface orientation. The Pt(111) sample was cleaned by argon ion sputtering and annealing at 1050 K in a vacuum. The sample was resistively heated, and the temperature was measured with a K-type thermocouple spot-welded to the rear side of the sample.

The ASW films were deposited at normal incidence to the Pt(111) at 100 K under conditions known to produce dense, relatively smooth ASW.[31−33] Crystalline ice samples were grown at 140 K. The water films covered the whole face of the sample. The area of the first monolayer (ML) peak in the temperature programmed desorption (TPD) spectra was used to calibrate the water coverage, θ. The estimated absolute uncertainty in the coverages is ±15%. The relative coverages are reproducible to ±10% between different experiments. The ASW films were irradiated with pulses of 87 or 1000 eV electrons with typical current densities of $\sim 2 \times 10^{12}$ electrons/cm^2/pulse, and beam spot sizes of ∼1.5 mm. The electron beam was incident at 45° to the sample normal. For these experiments, the electron beam irradiated a single spot on the sample (i.e., the beam was not scanned across the sample).

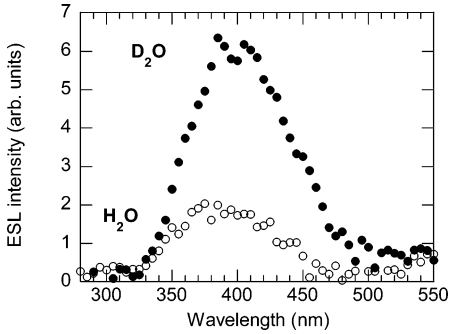

Figure 1. Electron-stimulated luminescence (ESL) spectra from 200 ML of D_2O (filled circles) and H_2O (open circles) amorphous solid water deposited on Pt(111) and irradiated with 87 eV electrons at 100 K. The double-peaked central feature seen in the spectrum for D_2O, which is reproducible, is similar to previous observations.

The electron-stimulated luminescence was measured with a photomultiplier tube (PMT) (Hamamatsu R2027) with spectral response in 160−820 nm range (maximum around 400 nm). Unless otherwise noted, the total emission yield was measured by positioning the PMT at normal incidence without passing it through a monochromator. A Bausch & Lomb grating monochromator with 675 grooves/mm and spectral range of 285−1400 nm was used to measure the emission spectrum. Since the luminescence signal is low, a 3 mm entrance slit and a 1 mm exit slit were used to increase the monochromator throughput, resulting in 16 nm spectral dispersion. The monochromator was calibrated with a Hg lamp standard. The luminescence signal is smaller than, and superimposed upon, the light emitted by the filament in the electron gun. To overcome this problem, the incident electron beam was pulsed (2 ms pulses at 100 Hz) by applying voltage to a suppression aperture in front of the filament, and the pulsed luminescence signal was acquired with a lock-in amplifier (SR-510, Stanford Research Systems).

III. Results and Discussion

Figure 1 shows the electron-stimulated luminescence spectra from 200 ML of D_2O (filled circles) and H_2O (open circles) amorphous solid water (ASW) deposited on Pt(111) and irradiated with 87 eV electrons at 100 K. The ESL intensity depends on the ASW film thickness, but the spectra are otherwise independent of the thickness. The spectra are centered near 400 nm with a full width at half-maximum of ∼100 nm. The D_2O spectrum has a barely resolved, but reproducible, double-peaked structure. The spectra are similar to the reported spectra for crystalline ices under electron irradiation,[15−24,26,27,34] and close to other reported spectra of X-ray stimulated luminescence of ices. The characteristic double-peaked shape was also found in the fluorescence spectrum of H_2O and D_2O vapor after UV excitation (E_γ > 10 eV).[30] Potential energy surface calculations suggested that the main part of the emission spectra is due to the $\tilde{C} \rightarrow \tilde{A}$ electron transition from a highly excited state to the dissociative, first excited state of water:[30]

$$H_2O(\tilde{X}) + \hbar\omega \rightarrow H_2O(\tilde{C}) \rightarrow H_2O(\tilde{A}) + \hbar\omega \rightarrow H + OH(X)$$

The complicated shape of the gas-phase emission spectrum is the result of several vibrational states of the OH, which effect the partial emission cross-sections.[30] The emission spectra for amorphous solid water and crystalline ice are blue shifted by

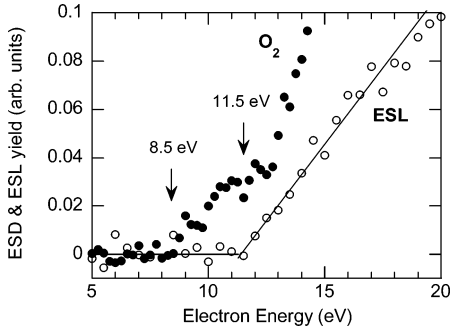

Figure 2. Integrated ESL emission yield (open circles) and O_2 ESD yield (filled circles) versus energy of incident electrons for 150 ML D_2O films deposited at 100 K. The data show onsets at 11.5 ± 0.5 eV for ESL and at 8.5 ± 0.5 eV for O_2 ESD.

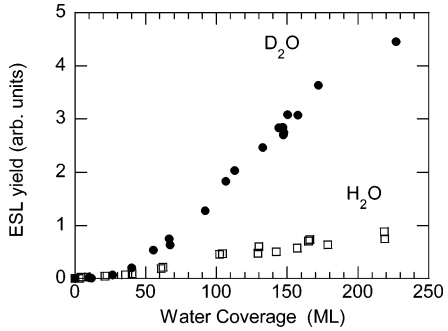

Figure 3. Integrated ESL yield versus ASW coverage for both D_2O (filled circles) and H_2O (open squares). The ESL yield was integrated during the first 10 s of irradiation. The luminescence yields are low for coverages <50 ML, and monotonically increase at higher coverages for both isotopes. The D_2O/H_2O ESL yield ratio is ~4−5 and approximately constant in the whole coverage range.

~50 nm compared to the gas-phase emission spectrum probably due to matrix effects on the $\tilde{C} \rightarrow \tilde{A}$ transition.[23] The H_2O and D_2O emission spectra look similar within our sensitivity and resolution limits (Figure 1), but the ESL yield from H_2O is ~3 times lower than that from D_2O. (As discussed below, the *initial* ESL yield from H_2O is ~4−5 times smaller. However, the H_2O ESL decays less with electron dose, and the spectra in Figure 1 are obtained after the ESL has decayed to its saturation value.) The lower yield for H_2O agrees with earlier observations for crystalline ices, and likely relates to more efficient quenching of excited states in H_2O via vibrational relaxation.[19,27]

If the ESL is primarily associated with the $\tilde{C} \rightarrow \tilde{A}$ transition in water, then the ESL threshold should occur at higher incident electron energy than the threshold for processes related to excitation of the lowest excited state. Figure 2 shows total ESL emission yield (i.e., measured without the monochromator) versus the incident electron energy. For these data, 150 ML D_2O films were deposited and irradiated at 100 K. The ESL yield has an apparent threshold at 11.5 ± 0.5 eV, which is close to the 11−12 eV thresholds reported earlier,[26,27] and similar to 11.4 eV estimated for $\tilde{X} \rightarrow \tilde{C}$ transition in ice.[23] We have also measured the O_2 ESD yield versus incident electron energy for 150 ML D_2O films. In this case, the apparent threshold is at 8.5 ± 0.5 eV. It is believed that the onset for the O_2 ESD corresponds to excitation of the lowest excited state in solid water,[35,36] which was measured in the ASW at 8.5 eV by EELS.[37] The ~3 eV shift between the ESL and ESD thresholds is very close to the photon energy at the maximum of the luminescence spectra (~400 nm), which supports the emitter assignment as the superexcited $\tilde{C}$ state. As discussed below, it is difficult to measure the ESL threshold versus electron energy from very thin ASW layers since the luminescence yield decreases dramatically. For thicker films (e.g. 150 ML), the measured threshold value may experience some systematic shift because of electron-induced charging of the film. However, decreasing the incident electron beam current and decreasing the film thickness to 100 ML did not change the apparent threshold within the uncertainty of the measurement. We believe the total charging is small primarily due to the fact that the ESD yields of D_2O and D_2 are constant versus time for thick ASW films (data not shown).

Above the threshold, the luminescence yield monotonically increases with increasing electron energy up to the highest energies investigated (E_i = 80 eV, data not shown). The increase of the ESL yield with electron energy indicates that in addition to direct excitation, ionization followed by electron−ion recombination also leads to formation of the excited states responsible for the luminescence. Since the luminescence comes from a superexcited state, the electron−ion recombination must occur on a time scale short compared to the relaxation time of the electron in the excited-state manifold.

The integrated ESL yields versus ASW coverage from 0 to ~220 ML for both D_2O and H_2O are shown in Figure 3. For these data, the monochromator was not used and the ESL yield was integrated over the first 10 s of irradiation. Similar results are obtained for other integration times. (The time/fluence dependence of the luminescence is discussed below.) For both isotopes, the luminescence yields are low for coverages less than 50 ML and increase approximately linearly with coverage thereafter. The yields begin to decrease for coverages above ~240 ML for both D_2O and H_2O (data not shown). The D_2O/H_2O ESL yield ratio is ~4−5 over the whole coverage range. The ESL versus coverage (Figure 3) is qualitatively similar to the luminescence of thin argon films under VUV irradiation.[13,38] In that case, the authors proposed a model in which migrating excitons could either decay via luminescence in the bulk or stimulate desorption if they reached the surface of the film. However, as discussed below, we believe that in water films the coverage dependence is due to interference and energy transfer effects with the substrate and is not related to exciton migration.

Previous experiments demonstrate that electron-stimulated reactions in thin films on Pt(111) occur at both the Pt/water and water/vacuum interfaces and that the total amount of electron-stimulated reactions, as measured for example by the total sputtering, is maximized for films of intermediate thickness (typically ~20−30 ML depending on the conditions of the experiment).[6−8] On the basis of these results, it would be useful to characterize the spatial distribution of ESL within the films to see if it also is correlated with reactions at the interfaces. To measure the spatial distribution of the ESL, we can utilize the dependence of the ESL yield on the water isotope (Figure 3). For example, Figure 4a shows the ESL signal from layered H_2O and D_2O ASW films versus the coverage of the H_2O or D_2O "cap" layer (i.e., the isotope deposited last). For these experiments, the total coverage is constant: $\theta_{D_2O} + \theta_{H_2O} = 155$ ML. For H_2O deposited on top (solid circles), the ESL signal decreases as the H_2O cap layer coverage increases, reaching a constant value for $\theta_{H_2O} >$ ~22 ML. Conversely, for D_2O deposited on top (open squares), the ESL signal increases with increasing D_2O coverage and saturates for $\theta_{D_2O} >$ ~35 ML. These results show that the ESL is localized in the outer 20−30 ML of the ASW films, depends on the isotope present in that region of the film, and is independent of the isotopic composition deeper within the film. In Figure 4b, we show the ESL yield from 30 ML of D_2O deposited on top of various amounts of H_2O versus the total coverage of the water film.

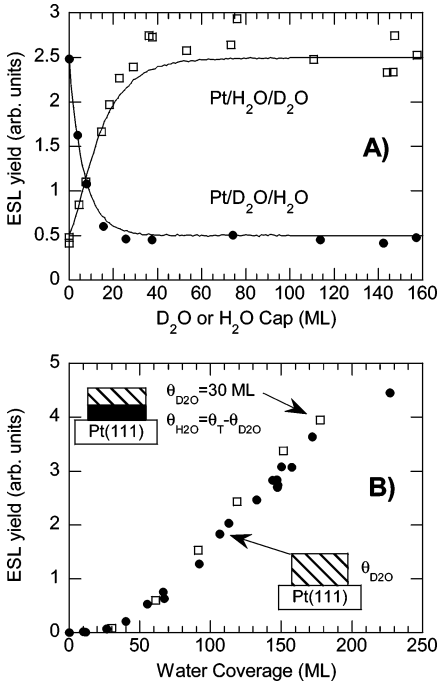

Figure 4. (A) Integrated ESL yield from the isotopically layered films $Pt/H_2O/D_2O$ (open squares) and $Pt/D_2O/H_2O$ (filled circles) versus the coverage of the D_2O or H_2O cap layer where the total water coverage, θ_T, is constant, $\theta_T = \theta_{D_2O} + \theta_{H_2O} = 155$ ML (i.e., the fraction of each isotopic layer is changed from 0 to 1). The lines are the results of a model discussed in the text (see also Figure 6). (B) ESL yield from a 30 ML of D_2O layer on top of an H_2O spacer versus the total water coverage (open squares). For reference, the ESL yields from pure D_2O films are also shown (filled circles). Both ESL yields versus coverage are practically identical.

Also shown for comparison is the ESL from pure D_2O versus D_2O coverage (from Figure 3). The ESL signal from 30 ML of D_2O on an H_2O spacer layer (squares) is essentially identical with the ESL signal from pure D_2O (circles) indicating that, for all coverages, the ESL emission is localized in the top ~20−30 ML of the ASW films.

The results in Figure 4 indicate that for 87 eV electrons most of the electron-stimulated luminescence originates from the outer 20−30 ML of the ASW films. In crystalline ice at 100 K, the distance between successive planes along the *c*-axis is 0.366 nm.[39] By using this distance for the ASW films to convert from coverage to thickness and taking into account the 45° angle of incident for the electrons, 20−30 ML corresponds to an electron penetration depth of ~10−15 nm. This distance is close to the penetration depth of ~5−10 nm calculated for 100 eV electrons in condensed water.[40] In this case, the "penetration depth" refers to the region where most of the electronic excitations are produced within the film. Since the films do not charge appreciably (vide supra), subexcitation electrons and/or mobile holes must migrate through the film.[41] Increasing the electron energy increases the penetration depth and increases the thickness of the layer from which the ESL is emitted: The integrated ESL yield from isotopically layered 250 ML ASW films irradiated with 1000 eV electrons increases versus the D_2O cap layer coverage (squares) until $\theta_{D_2O} \sim 100$ ML, and is constant at higher coverages (Figure 5). These data imply a penetration depth of ~50 nm for the incident electrons, which is close to the calculated value for 1000 eV electrons in condensed water.[40] In Figure 5, the results for 87 eV electrons irradiating a D_2O cap layer (i.e., Figure 4a) are also shown for comparison (circles).

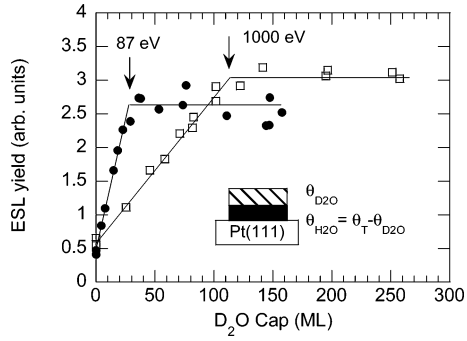

Figure 5. Integrated ESL yield from the isotopically layered films $Pt/H_2O/D_2O$ versus the D_2O cap layer coverage, θ_{D_2O}, for 87 eV incident electrons (filled circles) and for the 1000 eV incident electrons (open squares) where the total water coverage, θ_T, is constant: $\theta_T = \theta_{D_2O} + \theta_{H_2O} = 155$ and 250 ML, respectively. The results indicate that most of the ESL is emitted from the outer layer, close to the penetration depth of the incident electrons: ~10 and ~50 nm for 87 and 1000 eV electrons, respectively (taking into account the incident angle of the electrons).

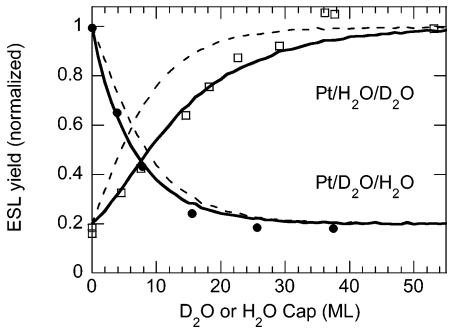

Figure 6. Integrated ESL yield from the isotopically layered films $Pt/H_2O/D_2O$ (open squares) and $Pt/D_2O/H_2O$ (filled circles) versus the coverage of the D_2O or H_2O cap layer where the total amount of ASW is constant (see Figure 4a). The lines show the results of modeling the ESL with energy transfer (solid lines) and without energy transfer (dashed lines) from the D_2O to the H_2O layers (see text for details).

Since the ESL from 87 eV electrons occurs only in the outer ~20−30 ML of a water film (Figure 4), we need to consider why the ESL yield increases with increasing coverage up to ~240 ML (Figure 3). It is likely that the rest of the film underneath the emitting layer serves as a dielectric spacer separating the emitting dipoles from the metal substrate and affecting the luminescence yield. In fact, similar distance-dependent fluorescence yields and lifetimes have been observed in many other metal−dielectric systems.[42,43] There are two main processes affecting the luminescence yield near metal surfaces:[42,43] First when the distance between an excited atom or molecule and the surface is considerably less than the wavelength of the emitted radiation, then nonradiative transfer of energy from the excited molecule to the metal tends to quench the luminescence. The nonradiative transfer is similar to dipole−dipole (Förster) energy transfer.[43] Second, destructive interference effects with the light reflected from the substrate reduce the luminescence for thicknesses comparable to the wavelength of the light.

The experiments with layered films of H_2O and D_2O show that the excited states responsible for the ESL do not migrate over distances that are large compared to the penetration depth of the incident electrons (Figure 4). However, these same experiments show an asymmetry depending on which isotope is deposited on top that is probably due to energy transfer or migration on a shorter length scale (Figure 6). Three features of the data highlight the asymmetry: First, the magnitude of

the initial slope of the luminescence signal versus cap layer coverage is different for the two cases. In particular, when H_2O is on top, the luminescence decreases approximately twice as quickly compared to the rate of increase when D_2O is on top. Second, the luminescence yield at the point where the data curves cross in Figure 6 is *less* than the average of the luminescence yields for pure D_2O and H_2O, i.e., the curves cross at ~0.43 instead 0.6. Third, for H_2O on top the luminescence saturates $\theta_{H2O} > \sim 22$ ML versus saturating at $\theta_{D_2O} > \sim 35$ ML for D_2O on top. If the isotopes were equal except for the luminescence yield (i.e., symmetric), the magnitude of the initial slopes would be the same, the luminescence curves would cross at the average value of yield for the pure films, and the luminescence would saturate at the same coverages (dashed lines, Figure 6).

The spatial distribution of electronic excitations is probably independent of the isotope.[44,45] Therefore, the data suggest that electronic excitations created in the D_2O layer can migrate to the H_2O layer and subsequently decay nonradiatively. To model the data, we can use a simple one-dimensional Monte Carlo simulation that takes into account the initial spatial distribution of the excitations, their subsequent diffusion, and luminescence or quenching. The energy deposition per unit length of primary electrons (i.e., electronic excitations and ionizations) in the film can be approximated by a Gaussian $I(x) = dE/dx = \exp[-(x - x_0)^2/2\sigma^2]$, where σ is the standard deviation and $I(x)$ is maximized at x_0.[40] To run a simulation, a cap layer thickness and isotope ordering (i.e., H_2O or D_2O on top) are specified. An initial location for an excitation is randomly chosen from the Gaussian distribution. For each Monte Carlo iteration, the excitation either takes a random walk step (i.e., diffuses), luminesces, or quenchs. So $P_{diff} + P_L + P_Q = 1$, where P_{diff}, P_L, and P_Q are the probabilities for diffusion, luminescence, and quenching, respectively. P_{diff}, P_L, and P_Q depend on the isotope at the current position of the excitation. Each excitation "trajectory" is followed until it luminesces or quenchs, and excitation "trajectories" are run until sufficiently good statistics are obtained for the luminescence yield for this configuration. The procedure is then repeated for each cap layer thickness and isotope ordering, to model the data in Figure 6.

The model has several parameters that need to be chosen. First, we use calculations of dE/dx for 100 eV electrons in water,[40] to determine σ and x_0: $\sigma = 6$ layers (~2.2 nm) and $x_0 = 0$. Note that almost any distribution with a similar length scale for the penetration depth of the beam will give qualitatively similar results. Second, the experimental ESL yield from pure D_2O is approximately 5 times greater than the ESL yield from pure H_2O (see Figures 3 and 4 for large cap layer coverages). This determines the ratio, R_{LQ}, of the luminescence to quenching probabilities for each isotope: $R_{LQ}(D_2O) = 5{:}1$ and $R_{LQ}(H_2O) = 1{:}5$. Therefore, since the probabilities must sum to one, there is only one independent probability for each isotope, and the model has two adjustable parameters. We adjust the diffusion probabilities, $P_{diff}(H_2O)$ and $P_{diff}(D_2O)$, and express them in terms of the average number of random walk steps, $N_{steps}(H_2O)$ and $N_{steps}(D_2O)$, an excitation in a pure film would make prior to either luminescing or quenching: $N_{steps} = (1 - P_{diff})^{-1} - 1$.

The solid lines in Figure 6 show the results of a simulation for $N_{steps}(H_2O) = 100$ and $N_{steps}(D_2O) = 300$, which qualitatively reproduces the data including the initial slopes, crossing point, and saturation values discussed above. The simulation suggests that for the pure D_2O (H_2O) films the typical distance (normal to the surface) between where an excitation is created and where it either emits or quenches is ~6 nm (~3.7 nm) corresponding to ~17 ML (~10 ML). For comparison, the dashed lines show the simulation results for the "symmetric" case where $N_{steps}(H_2O) = N_{steps}(D_2O) = 100$. As noted above, the σ used in the simulations is based on published reports. However, comparable fits to the data can be obtained for simulations with a larger penetration depth for the incident electrons (i.e., larger σ) and less diffusion of the electronic excitation. Therefore, the data and simulation do not allow us to unambiguously determine these two parameters. Other experiments measuring various electron-stimulated reactions versus coverage[6,8,46] suggest a somewhat larger penetration depth corresponding to $\sigma \sim 8-10$ layers. For simulations with σ in this range, the typical diffusion distances are somewhat smaller (~8−15 layers, depending on the isotope).

Energy transfer from D_2O to H_2O is consistent with X-ray radioluminescence experiments on homogeneous mixtures of H_2O and D_2O.[19] In those experiments, the luminescence yield was not proportional to the mole fraction-weighted yield of each isotope. Instead, the luminescence yield of isotopically mixed ice films was similar to the yield from pure H_2O films even for low concentrations of H_2O. Furthermore, the radioluminescence yield (at ~400 nm) of crystalline ice is significantly enhanced by the addition of some impurities in low concentrations (e.g., alkali halide salts at $\sim 10^{-3}$ mol/L).[15,19] The impurities may produce structural defects in the crystalline ice that promote luminescence. The observation that several different impurities at low concentrations affect the radioluminescence yields in similar ways is consistent with the hypothesis that the $\tilde{C}$-excitons are mobile.

The luminescence is primarily due to the emission from an electronically excited state of water (the $\tilde{C}$ state) that is formed either by direct excitation from the ground state or by electron−ion recombination. If the $\tilde{C}$ state is formed by electron−ion recombination, the recombination must happen on a time scale that is short compared to the relaxation time for an energetic electron in the excited-state manifold (e.g., the conduction band in crystalline ice), otherwise the resulting excited state would be lower in energy. The short time available would seem to preclude significant hole hopping. Therefore for both direct excitation and electron−ion recombination to form the $\tilde{C}$ state, it is probably the $\tilde{C}$ state that is mobile and is responsible for the energy transfer from the D_2O to the H_2O films. The experiments with layered films of H_2O and D_2O are insensitive to diffusion parallel to the surface. Therefore, a typical diffusion distance of 10 ML in one dimension should correspond to several hundred random hops for the exciton in three dimensions. (In the amorphous films there is no reason to expect a preferred direction for the excitons to diffuse.)

The relatively short-range migration of the $\tilde{C}$-excitons responsible for the ESL does not correspond to the much longer distances for the energy migration observed in the ESD experiments where energy transfer to the buried Pt/water interface can be observed over several hundred monolayers.[8] Therefore we do not believe that these highly excited states are involved in such long-range energy transfer. Nonetheless, the mobility of these high-energy excitons is noteworthy. Excitons in solids diffuse via correlated hopping of their electrons and holes. The exciton's range depends on the lifetime of the exciton and on its mobility. We expect the rate-limiting step to be the hole hopping step since the electronic wave functions associated with the hole are lower in energy and therefore more localized. The lowest energy exciton (corresponding to the lowest energy excited state in the gas phase) should have a longer lifetime

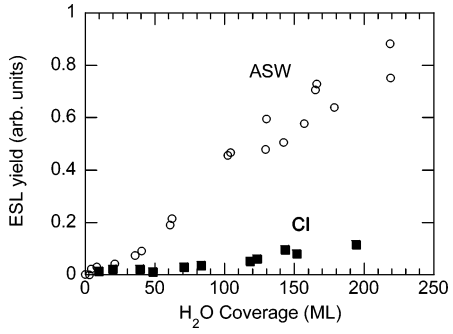

Figure 7. Integrated ESL yield versus coverage for amorphous (open circles) and crystalline (filled squares) films of H_2O on Pt(111). The amorphous (crystalline) films were grown at 100 K (140 K). The ESL yield from the crystalline films is ~6−7 times lower than the ESL yield from the amorphous samples.

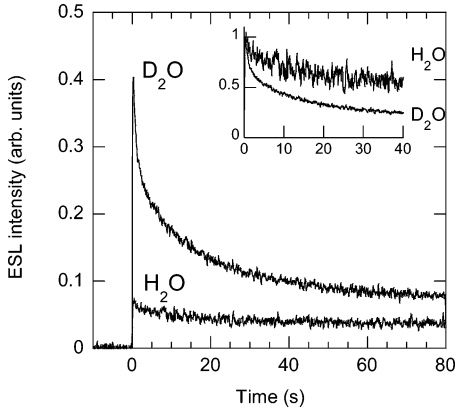

Figure 8. ESL yield versus irradiation time for 150 ML of amorphous D_2O and H_2O. The normalized emission dose-dependence is shown in the inset.

than the $\tilde{C}$-excitons. Therefore, since they share the same hole state,[47] it is reasonable to expect that the lower energy exciton can migrate further.

Figure 7 shows the ESL integrated yields versus coverage for amorphous (open circles) and crystalline ice (filled squares) films of H_2O on Pt(111). The ESL yield from the crystalline ice films is ~6−7 times lower than the ESL yield from the amorphous samples. Similar results are obtained for amorphous and crystalline D_2O films (data not shown). There are several possible explanations for the large differences in the ESL between crystalline ice and ASW. One possibility is that the excited electrons scatter less in the crystalline films thus traveling further from the hole and suppressing exciton formation via electron−ion recombination. The electron-stimulated reaction yields in water films, which involve electron−ion recombination, also depend on the phase (crystalline or amorphous) although the effect is not as strong. However, we believe that the ESD of neutral products such as atomic and molecular hydrogen and oxygen primarily involves lower energy excitons. In that case, the electron−ion recombination step might not be as sensitive to the phase. Another possibility is that the luminescence happens in the vicinity of some structural defects in the solid water network that has a higher concentration in the ASW films.

The radioluminescence yields in crystalline ice increase versus radiation fluence for 50 keV X-ray irradiation[15,18,19] and 0.5 MeV electron irradiation.[20] In these cases, the higher energy radiation may create defects in the crystalline ice that enhance the luminescence. In our experiments on ASW, the ESL yield from ASW decreases with increasing irradiation fluence. Figure 8 shows the ESL yield from 150 ML of amorphous D_2O and H_2O versus irradiation time. The ESL yield increases promptly when the electron beam is turned on, reaches a maximum after ~0.5 s, and then slowly decays approaching a steady state value on a scale of minutes (for the given beam current). After the e-beam is turned off, the ESL signal decays promptly to the base level.[48] If the irradiation is resumed, the ESL signal quickly returns to the level achieved at the end of the previous irradiation cycle. The normalized emission dose-dependence does not change with the ASW film thickness, but the ESL declines more slowly with increasing electron dose for H_2O (Figure 8, inset). The last two results suggest that charging of the ASW films during irradiation is not responsible for the ESL dose-dependence. Since the geometrical and electronic structures of the sites within the films where luminescence occurs are not known, a detailed explanation of the results in Figures 7 and 8 is not possible. One possibility is that, unlike high-energy irradiation of crystalline ice, low-energy electron irradiation of ASW "anneals" the film, removing defects that may be associated with the luminescence. In support of this, temperature programmed desorption spectra show that irradiated ASW films crystallize earlier in the temperature ramp than unirradiated films (data not shown). However, the ionizations and electronic excitations produced by the energetic electrons also create various reaction products (i.e., defects) in the ASW films. The spatial distribution of these radiolysis products within the film and their relationship to the ESL is unclear. For example, recent experiments suggest that low-energy, neutral excited states may dissociate only at the interfaces of the ASW films.[6,8] Since the ESL originates from within the penetration depth of the energetic electrons, reaction products accumulating at the interfaces may have only a small influence on the ESL. However, higher energy excitations may lead to dissociation within the films and the creation of defects. More research is necessary to identify the sites associated with the luminescence and the effects of various types of radiation on these sites.

IV. Conclusions

In summary, we have studied the low-energy electron-stimulated luminescence of thin films of D_2O and H_2O deposited on Pt(111). We find that the emission spectrum is centered at ~400 nm and the luminescence has a threshold at ~11.5 eV incident electron energy. The results are consistent with the assignment of the luminescence to the electronic transition in water molecule from the ground state to the superexcited state $\tilde{X} \rightarrow \tilde{C}$, followed by a radiative transition to the lowest excited state $\tilde{C} \rightarrow \tilde{A}$. The $\tilde{C}$ state is formed by both direct excitation and electron−ion recombination. The luminescence yield is suppressed by the metal substrate and increases with distance from the metal in the coverage range 0−200 ML. The electron-stimulated luminescence is emitted from the thin layer of the film at the vacuum side limited by the penetration of the incident electrons, corresponding to ~10 and ~50 nm for 87 and 1000 eV electrons, respectively. The electronic excitations responsible for the observed luminescence can migrate over a modest distance (~10 ML in H_2O) as shown by isotopic layering experiments. The emission yields from the amorphous solid water films are significantly higher than those from the crystalline water films, which may indicate involvement of structural defects in the emission process.

Acknowledgment. This work was supported by LDRD investments from PNNL. Pacific Northwest National Laboratory

is operated for the U.S. Department of Energy by Battelle Memorial Institute under contract DE-AC06-76RLO 1830.

References and Notes

(1) Farhataziz; Rodgers, M. A. J. *Radiation chemistry*: *principles and applications*; VCH Publishers: New York, 1987.
(2) Noell, J. O.; Melius, C. F.; Stulen, R. H. *Surf. Sci.* **1985**, *157*, 119.
(3) Rowntree, P.; Parenteau, L.; Sanche, L. *J. Chem. Phys.* **1991**, *94*, 8570.
(4) Kimmel, G. A.; Orlando, T. M. *Phys. Rev. Lett.* **1995**, *75*, 2606.
(5) Kimmel, G. A.; Orlando, T. M. *Phys. Rev. Lett.* **1996**, *77*, 3983.
(6) Petrik, N. G.; Kimmel, G. A. *Phys. Review Lett.* **2003**, *90*, 166102.
(7) Petrik, N. G.; Kimmel, G. A. *J. Chem. Phys.* **2004**, *121*, 3727.
(8) Petrik, N. G.; Kimmel, G. A. *J. Chem. Phys.* **2004**, *121*, 3736.
(9) Kimmel, G. A.; Orlando, T. M.; Vezina, C.; Sanche, L. *J. Chem. Phys.* **1994**, *101*, 3282.
(10) Kimmel, G. A.; Tonkyn, R. G.; Orlando, T. M. *Nucl. Instrum. Methods Phys. Res., Sect. B* **1995**, *101*, 179.
(11) Orlando, T. M.; Kimmel, G. A.; Simpson, W. C. *Nucl. Instrum. Methods Phys. Res., Sect. B* **1999**, *157*, 183.
(12) Song, A. K. S. *Self-trapped Excitons*; Springer-Verlag: Berlin, Germany; Heidelberg GmbH & Co. KG: Berlin, Germany, 1996.
(13) Reimann, C. T.; Johnson, R. E.; Brown, W. L. *Phys. Rev. Lett.* **1984**, *53*, 600.
(14) Shi, H.; Cloutier, P.; Gamache, J.; Sanche, L. *Phys. Rev. B*: *Condens. Matter* **1996**, *53*, 13830.
(15) Grossweiner, L. I.; Matheson, M. S. *J. Chem. Phys.* **1954**, *22*, 1514.
(16) Grossweiner, L. I.; Matheson, M. S. *J. Chem. Phys.* **1952**, *20*, 1654.
(17) Ghormley, J. A. *J. Chem. Phys.* **1956**, *24*, 1111.
(18) Steen, H. B. *Chem. Phys. Lett.* **1975**, *35*, 508.
(19) Steen, H. B.; Holteng, J. A. *J. Chem. Phys.* **1975**, *63*, 2690.
(20) Quickenden, T. I.; Trotman, S. M.; Sangster, D. F. *J. Chem. Phys.* **1982**, *77*, 3790.
(21) Quickenden, T. I.; Matich, A. J.; Bakker, M. G.; Freeman, C. G.; Sangster, D. F. *J. Chem. Phys.* **1991**, *95*, 8843.
(22) Freeman, C. G.; Quickenden, T. I.; Litjens, R. A. J.; Sangster, D. F. *J. Chem. Phys.* **1984**, *81*, 5252.
(23) Vernon, C. F.; Matich, A. J.; Quickenden, T. I.; Sangster, D. F. *J. Phys. Chem.* **1991**, *95*, 7313.
(24) Trotman, S. M.; Quickenden, T. I.; Sangster, D. F. *J. Chem. Phys.* **1986**, *85*, 2555.
(25) Miyazaki, T.; Nagasaka, S.; Kamiya, Y.; Tanimura, K. *J. Phys. Chem.* **1993**, *97*, 10715.
(26) Merkel, P. B.; Hamill, W. H. *J. Chem. Phys.* **1971**, *54*, 1695.
(27) Prince, R. H.; Sears, G. N.; Morgan, F. J. *J. Chem. Phys.* **1976**, *64*, 3978.
(28) Bernas, A.; Truong, T. B. *Chem. Phys. Lett.* **1974**, *29*, 585.
(29) Yada, T.; Norizawa, K.; Hirai, M.; Yamanaka, C.; Ikeya, M. *Jpn. J. Appl. Phys., Part 1* **2002**, *41*, 5874.
(30) Engel, V.; Mejer, G.; Bath, A.; Anderson, P.; Schinke, R. *J. Chem. Phys.* **1987**, *87*, 4310.
(31) Stevenson, K. P.; Kimmel, G. A.; Dohnalek, Z.; Smith, R. S.; Kay, B. D. *Science* **1999**, *283*, 1505.
(32) Kimmel, G. A.; Stevenson, K. P.; Dohnalek, Z.; Smith, R. S.; Kay, B. D. *J. Chem. Phys.* **2001**, *114*, 5284.
(33) Dohnalek, Z.; Kimmel, G. A.; Ayotte, P.; Smith, R. S.; Kay, B. D. *J. Chem. Phys.* **2003**, *118*, 364.
(34) Jones, W. M. *J. Chem. Phys.* **1952**, *20*, 1974.
(35) Orlando, T. M.; Sieger, M. T. *Surf. Sci.* **2003**, *528*, 1.
(36) Sieger, M. T.; Simpson, W. C.; Orlando, T. M. *Nature* **1998**, *394*, 554.
(37) Michaud, M.; Cloutier, P.; Sanche, L. *Phys. Rev. A* **1991**, *44*, 5624.
(38) Reimann, C. T.; Brown, W. L.; Johnson, R. E. *Phys. Rev. B* **1988**, *37*, 1455.
(39) Petrenko, V. E.; Whitworth, R. W. *Physics of Ice*; Oxford University Press Inc.: New York, 1999.
(40) LaVerne, J. A.; Pimblott, S. M. *J. Phys. Chem. A* **1997**, *101*, 4504.
(41) Prince, R. H. *Phys. Status Solidi B* **1976**, *78*, 271.
(42) Chance, R. R.; Prock, A.; Sibley, R. *Adv. Chem. Phys.* **1978**, *37*, 1.
(43) Waldeck, D. H.; Alivisatos, A. P.; Harris, C. B. *Surf. Sci.* **1985**, *158*, 103.
(44) Jonah, C. D.; Chernovitz, A. C. *Can. J. Phys.* **1990**, *68*, 935.
(45) Experiments indicate that the distance subexcitation energy electrons—those with energies below the threshold for electronic excitations—travel does depend on the isotope (ref 44).
(46) Petrik, N. G.; Kimmel, G. A. *J. Chem. Phys.* **2004**, submitted for publication.
(47) Tsurubuchi, S. *Chem. Phys.* **1975**, *10*, 335.
(48) A significant part of the signal rise/fall time in these experiments is associated with the electron-gun's current settling time (~0.2 s).